IEEE Access
Multidisciplinary | Rapid Review | Open Access Journal

Received 24 May 2023, accepted 1 July 2023, date of publication 18 July 2023, date of current version 31 July 2023.

Digital Object Identifier 10.1109/ACCESS.2023.3296599

RESEARCH ARTICLE

Double Negative (DNG) Metamaterial-Based Koch Fractal MIMO Antenna Design for Sub-6-GHz V2X Communication

FATIMA EZ-ZAKI[1], HASSAN BELAHRACH[1,2], ABDELILAH GHAMMAZ[1], SAROSH AHMAD[3,4], (Student Member, IEEE), ASMA KHABBA[5], KHAOULA AIT BELAID[1], ADNAN GHAFFAR[6], AND MOUSA I. HUSSEIN[7], (Senior Member, IEEE)

[1]Laboratory of Electrical Systems, Energy Efficiency and Telecommunications, Faculty of Sciences and Technology, Cadi Ayyad University, Marrakesh 40000, Morocco
[2]Royal School of Aeronautics, Marrakesh 40150, Morocco
[3]Department of Signal Theory and Communications, Universidad Carlos III de Madrid, Leganés, 28911 Madrid, Spain
[4]Centre de Energie, Matériaux, Télécommunication, Institut de la recherche scientifique (INRS), Montérial, Québec, H2X 1E3, Canada
[5]Instrumentation, Signals and Physical Systems (I2SP) Team, Department of Physics, Faculty of Sciences Semlalia, Cadi Ayyad University, Marrakesh 40000, Morocco
[6]Department of Electrical and Electronic Engineering, Auckland University of Technology, Auckland 1010, New Zealand
[7]Department of Electrical Engineering, United Arab Emirates University, Al Ain, United Arab Emirates

Corresponding authors: Sarosh Ahmad (saroshahmed@ieee.org) and Mousa I. Hussein (mihussein@uaeu.ac.ae)

ABSTRACT This paper presents the design an study of a DSRC/sub-6 GHz Koch fractal antenna single, two and four elements integrated with metamaterial structures, are proposed for the C-V2X and IEEE 802.11p/V2X. The design of automotive antenna is a challenging task due to the degradation of the MIMO antenna performance because of mutual coupling and cause spectral regrowth. Initially, a single antenna exhibits very good performance at 5.9-GHz. Subsequently, two elements and four MIMO elements were designed and analyzed which are placed orthogonally at the corner of the substrate introducing a diversity polarization. Meanwhile, to overcome the mutual coupling effects and improve the isolation between the radiating elements, two new different shaped left-handed metamaterials based on broadside and electrically coupled square split-ring resonator (SRR) with negative permeability and negative permittivity are suggested and their reflection properties are analyzed. However, the performances of various MIMO antenna configurations are investigated before and after inserting the metamaterial structures to assess the potential enhancements achieved. Finally, a further investigation concentrates on the effects of these metamaterial structures on the MIMO antenna radiation pattern and surface current density. In summary, the study demonstrated through simulations and measurements that the suggested MIMO antenna configurations, with the integration of metamaterial structures, exhibit improved performance, achieving a mutual coupling of -45 dB and demonstrating good MIMO diversity attributes

INDEX TERMS Koch fractal, DNG metamaterial, MIMO antenna, V2X communication, mutual coupling.

I. INTRODUCTION

Intelligent transportation systems (ITSs) that aim to improve transport safety and efficiency, low-latency, high-reliability, high-speed, and secure communication in a high-speed, congestive and dynamic environment, such as a solution for vehicle road collaboration by including novel applications, services, and technologies [1]. ITSs is based on the Vehicular ad Hoc Networking (VANETs) and consider a group of technologies that allow vehicles to share information and talk to each other as well as with the infrastructure, besides to provide the driver with various information about roadway conditions, reporting accidents and traffic jams, collision safety distance, gas stations, driver assistance including

The associate editor coordinating the review of this manuscript and approving it for publication was Tariq Umer.

parking, rest location, cruise control and so on [2], [3]. However, ITSs also cover the use of Information and Communication Technologies (ICT) for rail, water, and air transport including navigation systems. The main technologies used for vehicular communications around the world include Dedicated Short Range Communication (DSRC) and Cellular Vehicle to Everything (C-V2X) [1] as explained in Fig.1. DSRC based on IEEE 802.11p has standards well established in almost world countries in the range of 5 GHz due to the spectral environment and propagation characteristics [1], [2]. Therefore, in Europe, the European Telecommunications Standards Institute (ETSI) has allocated 30MHz of the spectrum in the 5.8 GHz band for DSRC in 2008 whilst the FCC reserved around 75 MHz in the 5.9 GHz band. Such connected vehicle networking lies in On-Board Units (OBU) installed in the vehicle as well as fixed Road Side Units (RSU) placed in a spot of the infrastructure [2], [3], [4]. As it is well known that the antenna plays a decisive role in achieving high performance of wireless communication system. Therefore, it is a great challenge to develop an automotive antenna module that provides various services, whereas maintaining high technical performances and good aesthetic aspects. However, most of the antenna designs that have been used in the recent ITS systems can be considered as conventional antenna models with a single antenna element, such as wire monopole/dipole, printed monopole/dipole, or PIFA. Nevertheless, the V2X communications systems suffer from such limitations due to the multipath fading environment and weaker signal in the process of data transmission caused by surrounding buildings, trees, and other vehicles [5]. To overcome this problem, multiple-input multiple-output (MIMO) systems use multiple antennas at the transmitter and receiver side respectively are used. They permit to achieve high data rates and throughput, to enhance the capacity of a wireless radio channel, and reduce the effect of fading [6], [7], [8], [9]. The MIMO performance can be further enhanced by exploiting the spatial and/or polarization diversity. On other hand, MIMO antenna which is able to reconfigure their radiation performance, with a high end of coverage, high gain, better signal-to-noise ratio, and fewer channel losses are becoming more and more suitable candidates in order to get the more improved features for automotive applications [5], [6], [7], [8], [9], [10], [11]. One of the most important tracks of MIMO fractal antennas is their self-similar and space-filling behavior. Therefore, Fractal MIMO antenna arrays are inherently self-similar, self-affine, and have space-filling characteristics those permit to provide an enhanced bandwidth, better radiation pattern, low correlated signals [12], [13]. In this concept, various types of MIMO antenna fractal arrays such as Sierpinski geometries [14], [15], [16], Hilbert curve [17], [18], Minkowski [18], [19], Koch [20], [21], [22], and Cantor [23], [24] have been reported to achieve miniaturization, wide bandwidth and multiband characteristics. Other MIMO antenna designs have been proposed in [25], [26], for multiple applications. It is known that the very low mutual coupling between MIMO antenna elements is highly desirable for efficient MIMO system performance. In this regard, several techniques are used to eliminate the undesirable effect of this coupling as well presented in [27] and [28]. Using metamaterial structure is one of the very promoting method. Furthermore, metamaterials are considered artificial materials with unnatural electromagnetic properties such as negative permittivity and permeability. In other words, a negative refractive index (n) of those materials is named a double negative [28], [29]. These properties lead to backward wave propagation and these materials are known as left-hand materials [30], [31]. It is worth noting that the metamaterial electromagnetic properties are controlled by the structure of the design. Metamaterial structures can effectively provide a stop band at specific frequencies regarding the design structure. This feature has been used in order to reduce the mutual coupling between the radiating elements on a MIMO antenna system. Various kinds of the metamaterial designs have been performed in literature [32], [33], [34]. Although utilizing the metamaterial solution enables one to interrupt the surface current associated to the mutual coupling between the MIMO antenna elements, hence to improve the isolation and diversity performance of the system [35].

In the literature, the sub-6 GHz vehicular communication spectrum for 5G is of great interest in academia and industry due to its high data rate and high spectrum efficiency. Hence, the operating frequency band (from 2.5 GHz to 5.9 GHz) is the main sub-6 GHz frequency band for V2X communications. For a successful implementation of sub-6 GHz 5G standards, the antenna of multiple-input multiple-output (MIMO) systems is an important design consideration.

For instance, the target of the work at hand was the synthesis and investigation of multiple MIMO antenna configurations based on single Koch fractal antenna element properties to achieve a significant diversity performance and bandwidth enhancement with dual-polarization and enhanced diversity performance. The novelty of the proposed antenna configuration is to mitigate the mutual coupling and enhancing the diversity performance by introducing two new double negative (DNG) metamaterial structures on either side of the FR4 substrate. The basic element of the projected configurations is the Koch fractal patch antenna of the third iteration. The design and simulation of the proposed antennas are carried out using CST microwave studio using a time-domain solver. Thereby, the single antenna element is studied in section I. Whilst, the 2 × 1 MIMO antenna is given in section II. Section III will cover the detailed design of the 2 × 2 MIMO with and without DNG metamaterial cells along with the diversity analysis. The conclusion of the study is given in Section IV.

II. SINGLE ELEMENT DESIGN

A. PROPOSED ANTENNA DESIGN

The Koch fractal geometry is generated in the following steps. In the zeroth iteration, a line of length Lf is considered, in the first iteration, the length Lf is divided into three equal parts.

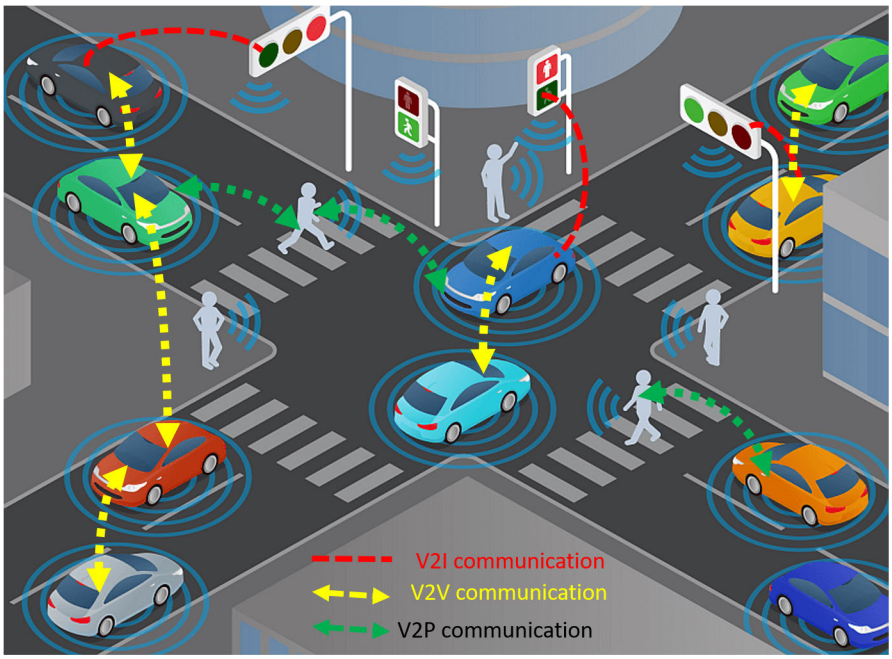

FIGURE 1. Vehicular network architecture cellular and DSRC.

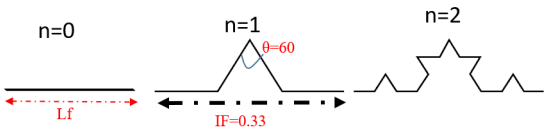

FIGURE 2. Koch geometry.

Then, the central part is formed by combining two identical slices, which form an equilateral triangle. In the second iteration, each sub-length ($Lf/3$) is divided into 3 equal parts. The process is repeated in consecutive iterations multiple times to construct the Koch curve. Furthermore, the Koch fractal is placed along the sides of an equilateral triangle.

Koch standard geometry (Fig.2) is characterized by two main factors: the iteration factor ($r = IF = 1/3$) which represents the construction law of fractal generation, and the iteration order ($n = 2$) which describes how many iteration processes are performed. This procedure is slow and complicated and to avoid these design complications, the fractal is generated using an easily implemented algorithm in MATLAB based on the generation rule defined by an IFS (Iterative Function System) approach based on the application of a series of affine transformations, w, given by (1):

$$w\begin{bmatrix} x \\ y \end{bmatrix} = \begin{bmatrix} a & b \\ c & d \end{bmatrix} \times \begin{bmatrix} x \\ y \end{bmatrix} + \begin{bmatrix} e \\ f \end{bmatrix} \tag{1}$$

Here a, b, c, and d are control rotation and scaling, while e and f are control linear translation on the x-axis and y-axis respectively [12], [29]. For the dominant mode of the cavity model of the equilateral triangle patch, the resonant frequency is defined as (2) and (3).

$$\begin{cases} a = \dfrac{1}{r}\cos(\theta) \\ b = \dfrac{1}{r}\sin(\theta) \\ c = \dfrac{1}{r}\cos(\theta) \\ d = \dfrac{1}{r}\sin(\theta) \end{cases}$$

$$f_{(m,n,p)} = \frac{2c}{3s\sqrt{\epsilon_r}}\left(m^2 + n^2 + p^2\right) \tag{2}$$

$$f_{(1,0)} = \frac{2c}{3s\sqrt{\epsilon_r}} \tag{3}$$

where:
f_r =5.9 GHz is the resonant frequency, ϵ_r is the substrate dielectric constant, c is the velocity of light, (m, n, p) are mode-defining integers and s is the triangle sides initial length. It is worth reminding that applying the Koch geometry to the equilateral triangle patch increases its electrical path length by increasing s and thus the fractal length decreases the resonant frequency. The single antenna element designed operating at 5.9 GHz for DSRC and C-V2X communication is printed on a 1.6 *mm* thick FR-4 substrate with permittivity of $\epsilon_r = 4.4$, and dimensions of $40 \times 40\ mm^2$. The geometrical stepwise evolution of the designed snowflake Koch antenna along with defected ground plane is shown in Fig.1. Initially, a snowflake Koch patch fed by a 50Ω microstrip line is feed by 50Ω microstrip lines with a tuning stub (Lf, Wf) and a partial ground plane ($W \times L_g$ is used (Antenna 2). Then,

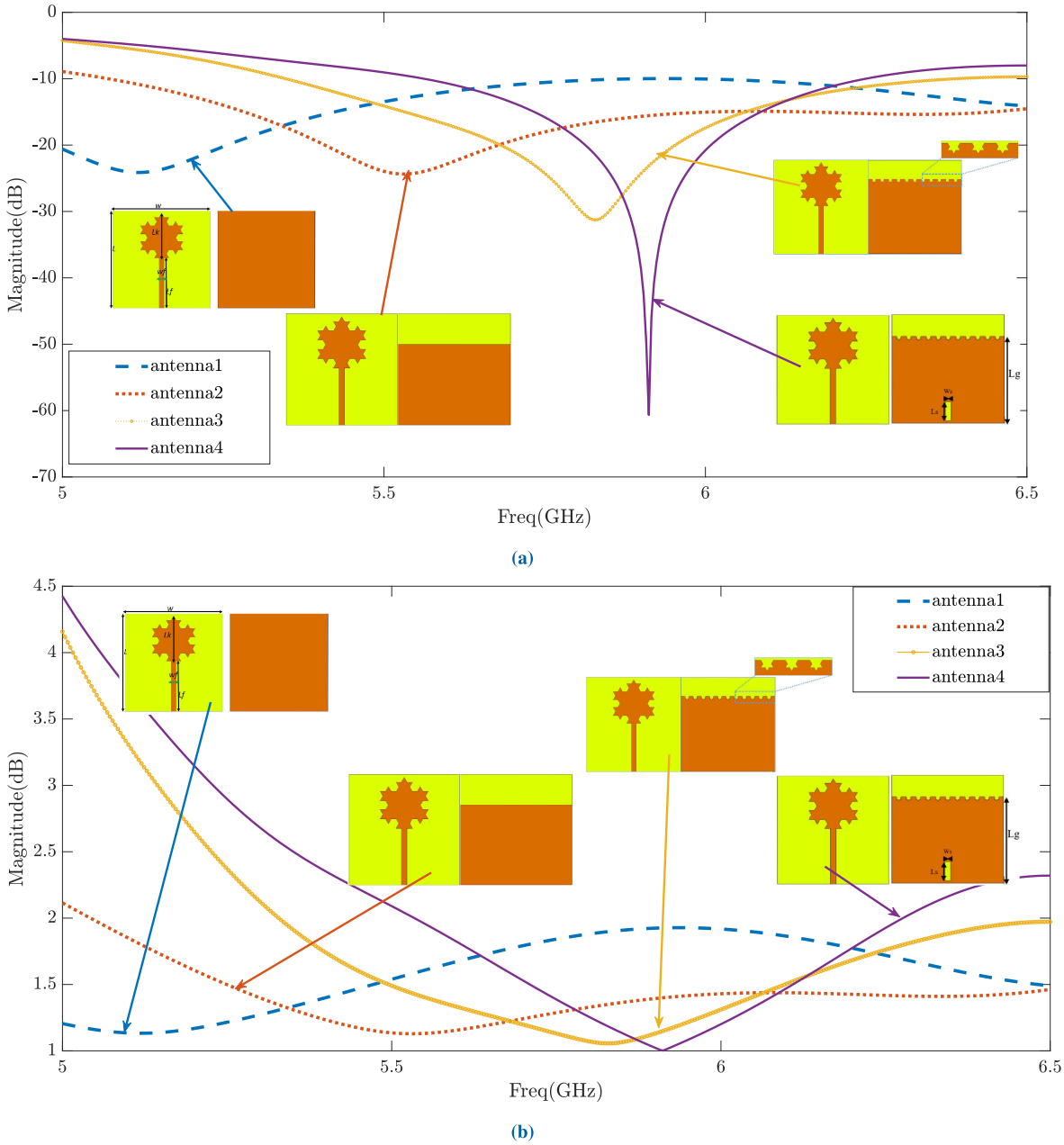

FIGURE 3. (a) variation of the S11 (dB) and (b) VSWR for the stepwise evlution of the proposed antenna.

a small Koch curve is etched from the ground plane's upper edge to achieve range as shown for Antenna 3. Furthermore, for achieving high impedance bandwidth, multiple defects in the ground plane are created using a square slot under the fed line which provides an improvement in matching conditions (Antenna 4). The proposed antenna involves a parametric analysis and optimization process using CST MWS software. The optimized dimensions of the proposed antenna are: $L = W = 40mm$, $h = 1.6\ mm$, $Lg = 32mm$, $Lk = 12mm$, $Wf = 2mm$, $Lf = 20.5\ mm$, $Ls = 7mm$, and $Ws = 2mm$. The comparison of the simulated reflection coefficient S11 in dB is demonstrated in Fig.3a. One can note that antenna 1 provides 2 bands but not the desired one, the antennas 2, 3, and 4 provide 3 bands including the desired band around the 5.9 GHz. It can be denoted that the proposed antenna 4 has a better reflection coefficient characteristic at the 5.9 GHz band as compared to Antenna 2 and Antenna 3. One can conclude that the antenna provides good impedance behavior and scattering parameters due to the etched slot and Koch curve on the partial ground structure. VSWR is an image of impedance matching of the simulated proposed antenna stepwise evolution (Fig.3b). It can be seen that the antenna presents a very good impedance matching represented with a VSWR less than 2 over the operating band. Moreover, the

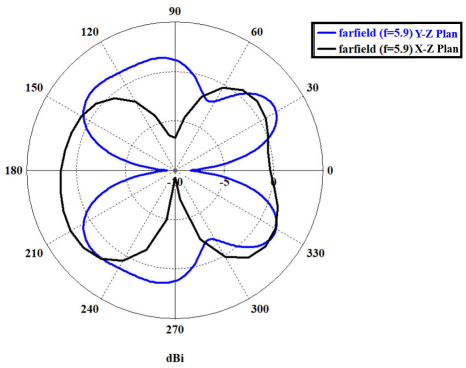

FIGURE 4. Antenna radiation pattern in XZ-Plane(black line) and YZ-plane(Blue line).

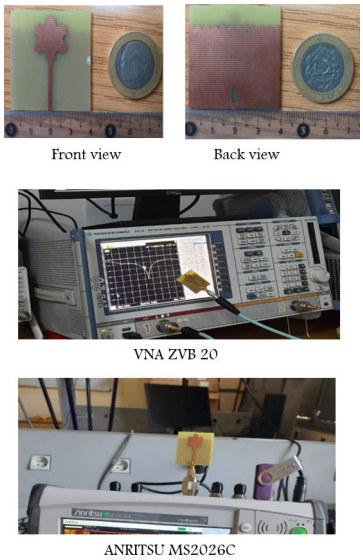

FIGURE 5. The designed single Koch antenna prototype.

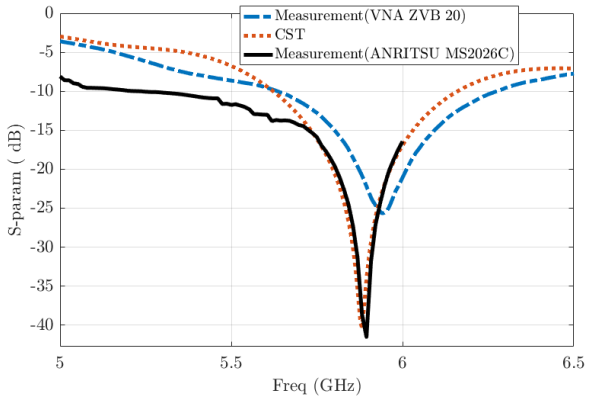

FIGURE 6. Simulated and measured S-parameters comparison.

proposed antenna reaches a bidirectional radiation patterns in the XZ plane and YZ plane respectively. In addition, the radiation patterns have low levels of cross-polarization and a symmetric form at 5.9 GHz as projected in Fig.4. It is

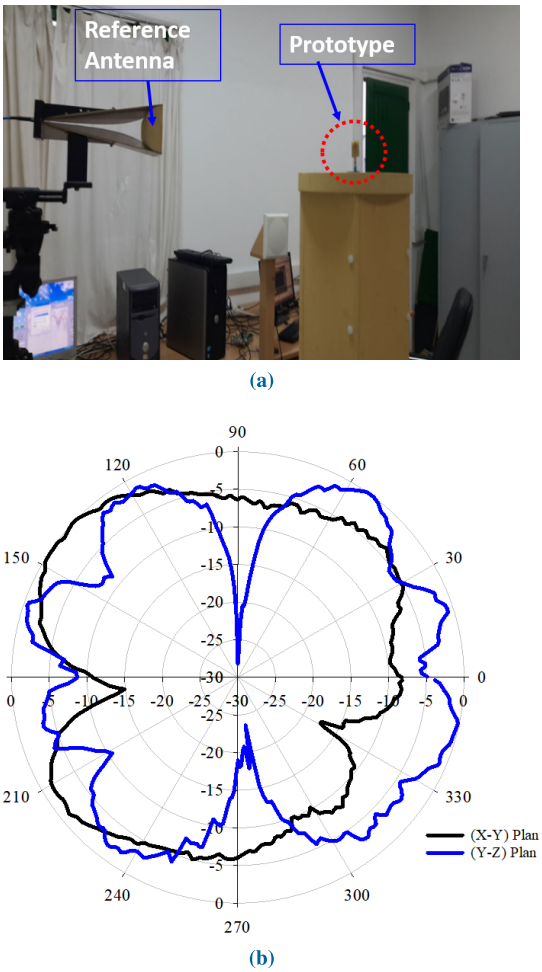

FIGURE 7. (a) The experimental setup, (b) Measured radiation pattern.

observed that the etching of rectangle slot and Koch curves on the ground plane make a significant impact on the antenna features. The final design provides an excellent value of the reflection coefficient (the reflection coefficient S11 is higher than -50 dB) as well as the VSWR of 1.023 for the DSRC band which means that the proposed antenna design is properly matched and represents a very good candidate for the V2X communication as well as for other standards.

B. PROPOSED ANTENNA MEASUREMENT

To validate the proposed single-element antenna structure, a prototype was fabricated and characterized. The photo of the prototype as well as the measurement set up are shown in (Fig.5). The measurement of the fabricated antenna was performed using an ANRITSU MS2026C vector network analyzer operating in the frequency range of 10 kHz to 6 GHz. These measurements were also repeated using another vector network analyzer, ZVB 20, operating in the frequency range of 10 MHz to 20 GHz. (Fig.6) shows the measured and simulated reflection coefficient of the proposed fractal antenna. As we can observe, there is good agreement between the simulated and measured resonance frequencies, despite a

slight increase in the reflection coefficient toward higher frequencies for the measurements taken with the ZVB 20 VNA. The difference between the two graphs is due to measurement uncertainties. The radiation pattern measurements were performed, as shown in (Fig.7a)). The normalized radiation patterns measured in the XY and YZ planes at 5.9 GHz are depicted in (Fig.7b). These measurement results allow us to clearly observe the variations in the radiation pattern of the fabricated antenna prototype at the resonance frequency of 5.9 GHz. In the XY plane, we can see that the radiation pattern of the proposed antenna tends towards an omnidirectional shape with slight degradation due to measurement uncertainties. In the YZ plane, the radiation pattern tends towards a bidirectional shape. However, we can observe that the radiation pattern in this YZ plane shows small variations due to reflections on the edges of the fractal antenna structure and also due to the surrounding measurement environment.

III. MIMO DIVERSITY ANALYSIS

The performance of the MIMO antenna entirely depends on diversity performance. This diversity performance is evaluated by some parameters that include envelope correlation coefficient (ECC), mean effective gain (MEG), diversity gain (DG), and total active reflection coefficient (TARC), and CCL (channel capacity loss). The ECC describes the correlation between the radiating elements of a MIMO antenna. Ideally, the ECC should be zero, but anything less than 0.5 is acceptable in a practical sense. It explores how the radiating element provides interference to another element of the system during excitation. It can be calculated by either using S-parameter value or using radiation pattern. Equations (4) derives ECC using S-parameter.

$$ECC_{(i,j)} = \frac{\sum_{n=0}^{N} \left| S_{i,n}^{*} S_{n,j} \right|^{2}}{\prod_{k=i,j} \left(1 - \sum_{n=1}^{N} S_{k,n}^{*} S_{n,k} \right)} \tag{4}$$

Diversity gain (DG) derives using equation (5) is another important diversity parameter, it is very powerful to measure the signal-to-noise ratio of the MIMO antenna. The diversity gain magnitude should be around 10, but practically more than 9.5 is acceptable.

$$DG = 10\sqrt{1 - |ECC|^{2}} \tag{5}$$

The mean effective gain (MEG) is another important performance analyzer for the multiple antenna system. The power intensity between the signals from each radiator of a MIMO antenna is evaluated using MEG. It also analyzes the antenna performance in adverse environmental conditions. The MEG performance of a MIMO antenna is calculated using the S-parameter of the specified antenna mentioned in Eq.6, Eq.7, and Eq.8. Where i is the exciting port and j denotes the other terminated ports of the antenna. Good isolation performance is obtained when the k value does not exceed $3dB$.

The overall isolation performance of the MIMO antenna is also expressed in the term of total active reflection coefficient (TARC) curves. It simply reflects the ratio between reflected and incident power. It derives the effective operating bandwidth of a MIMO antenna system. The operating bandwidth of the TARC is observed here with the variation of input phase from 0° to 180° with a 30° step size. The operating bandwidth ($-10dB$) at all phase angles should cover the desired frequency band. The total active reflection coefficient (TARC) is calculated using the S-parameter values of the proposed antenna according to Equations (9)-(10) for 2 ports and 4 ports MIMO antenna respectively, where θ, θ', θ'' are the excitation phase angles of the input feeding ports.

$$MEG_i = 0.5\left(1 - \left|S_{i,i}\right|^{2} - \left|S_{i,j}\right|^{2}\right) \tag{6}$$

$$MEG_j = 0.5\left(1 - \left|S_{j,i}\right|^{2} - \left|S_{j,j}\right|^{2}\right) \tag{7}$$

$$MEG = k = \left|MEG_i - MEG_j\right| \tag{8}$$

$$TARC_{2ports} = \frac{\sqrt{\left|S_{1,1} + S_{1,2}e^{j\theta}\right|^{2} + \left|S_{2,1} + S_{2,2}e^{j\theta}\right|^{2}}}{\sqrt{2}} \tag{9}$$

$$TARC_{4ports} = \frac{\sqrt{\begin{array}{l}\left|S_{1,1} + S_{1,2}e^{j\theta} + S_{1,3}e^{j\theta'} + S_{1,4}e^{j\theta''}\right|^{2} \\ + \left|S_{2,1} + S_{2,2}e^{j\theta} + S_{2,3}e^{j\theta'} + S_{2,4}e^{j\theta''}\right|^{2} \\ + \left|S_{3,1} + S_{3,2}e^{j\theta} + S_{3,3}e^{j\theta'} + S_{3,4}e^{j\theta''}\right|^{2} \\ + \left|S_{4,1} + S_{4,2}e^{j\theta} + S_{4,3}e^{j\theta'} + S_{4,4}e^{j\theta''}\right|^{2}\end{array}}}{\sqrt{4}} \tag{10}$$

Further investigation on channel capacity, is channel capacity loss (CCL) which must be specified in a rich multipath environment. It allows reliable communication over channel for a channel capacity loss (CCL) < 0.4 bits/s/Hz. The CCL value can be computed employing equation (11).

$$CCL = -\log_2 \times Det \begin{bmatrix} \rho_{1,1} & \cdots & \rho_{1,N} \\ . & . & . \\ \rho_{N,1} & .. & \rho_{N,N} \end{bmatrix} \tag{11}$$

where, N is the element number and $\rho_{i,i}$ and $\rho_{i,j}$ are defined as following:

$$\rho_{i,i} = 1 - \sum_{j=1}^{N} \left|S_{i,j}\right|^{2} \tag{12}$$

$$\rho_{i,j} = -\left(S_{i,i}^{*} S_{i,j} + S_{j,i}^{*} S_{j,j}\right) \tag{13}$$

IV. TWO ELEMENTS MIMO ANTENNA RESULTS ANALYSIS

A two elements MIMO is designed (Fig.8), simulated using CST Studio Suite as depicted in Fig.9. Meanwhile, to verify the accuracy of the simulated results, a fabricated prototype of the proposed two elements antenna is illustrated in Fig.10.

The S-parameters of the fabricated antenna prototype were measured by an ANRITSU MS2026C vector network analyzer with a range frequency of 500 kHz to 6 GHz. The

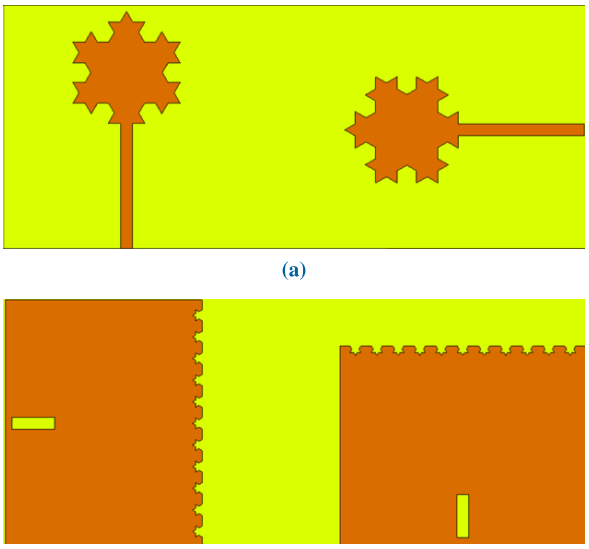

FIGURE 8. Proposed antenna: (a) Front view, (b) Back view.

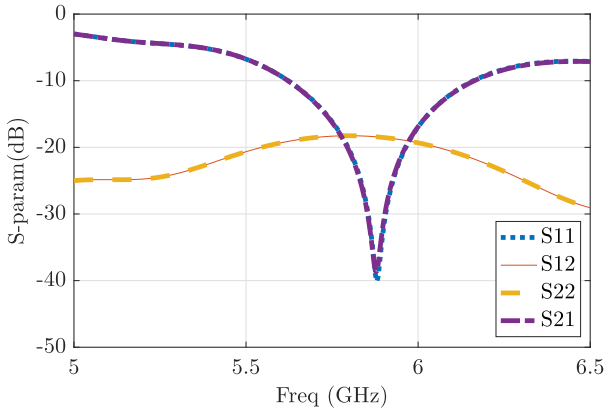

FIGURE 9. Antenna simulated S-parameters.

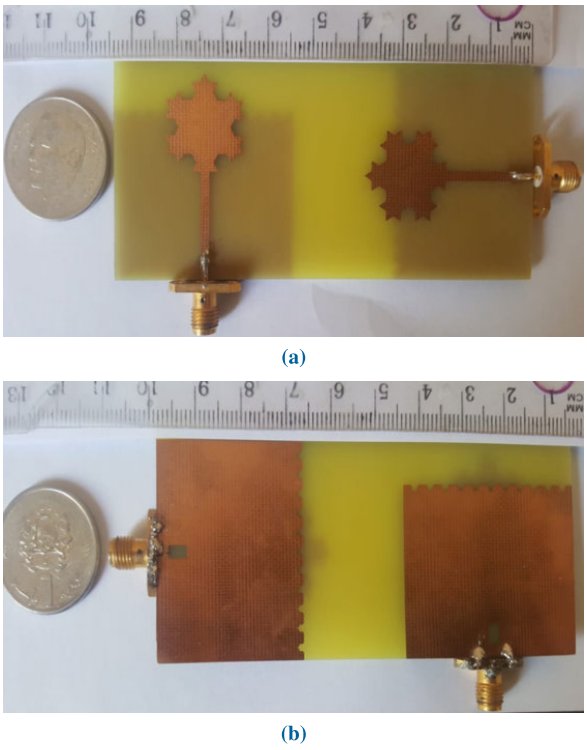

FIGURE 10. Antenna Prototype: (a) Front view, (b) Back view.

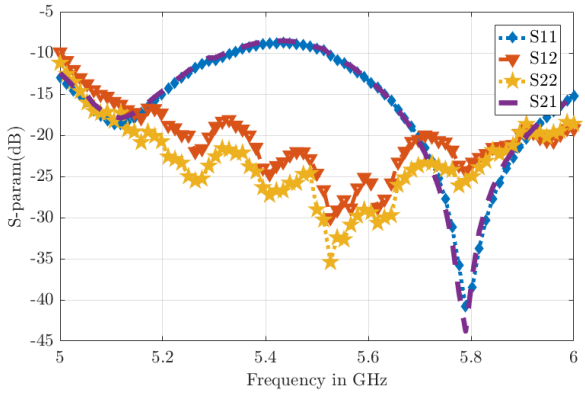

FIGURE 11. Measured S-parameters of the proposed antenna.

measured S-parameter are given in Fig.11. It is clear that, the impedance bandwidth (<-10dB) for simulated S11/S22 operates from 5.62 GHz to 6.16 GHz, while the measured one operates from 5.52 GHz to over 6 GHz. Also, it can be seen that measured and simulated S11/S22 have one resonance at 5.8 GHz and 5.9 GHz, respectively. However, the main resonance of the measured S11/S22 is shifted from that of the simulated one by about 100 MHz. Whilst, the measured S12/S21 have the same values as the simulated ones at 5.9 GHz. Whereas the measured results S12/S21 are also 7 dB lower than the one simulated at 5.8 GHz. It can be concluded that the fabricated prototype operates at 5.8 GHz, a bandwidth of 480MHz, besides the mutual coupling of the antenna is lower than -24 dB. It is worthwhile to note that the shifting between simulation and measurement is because of tolerances in the soldering and manufacturing of the connector, the quality of the substrate, the fabrication process, and losses in the long coaxial cable used in the process of measurement. Furthermore, the performance of the proposed MIMO antenna system is quantitatively evaluated by means of analyzing the envelope correlation coefficient (ECC), the diversity gain (DG), the total active reflection coefficient (TARC), and channel capacity loss (CCL). Moreover, for the attractive MIMO system, the value of ECC should be lower than 0.5, whilst the DG value should be close to 10, TARC lower than 0 dB, and CCL must be lower than 0.4 b/s/Hz. The corresponding ECC results are plotted in Fig.12a. The simulated ECC is lower than 0.005 within the operating bandwidth, while the measured values of ECC are observed to be below 0.01 for the operating frequency band with a peak value of 0.008 at 5.8 GHz. Low ECC value indicates that the investigated MIMO antenna can provide

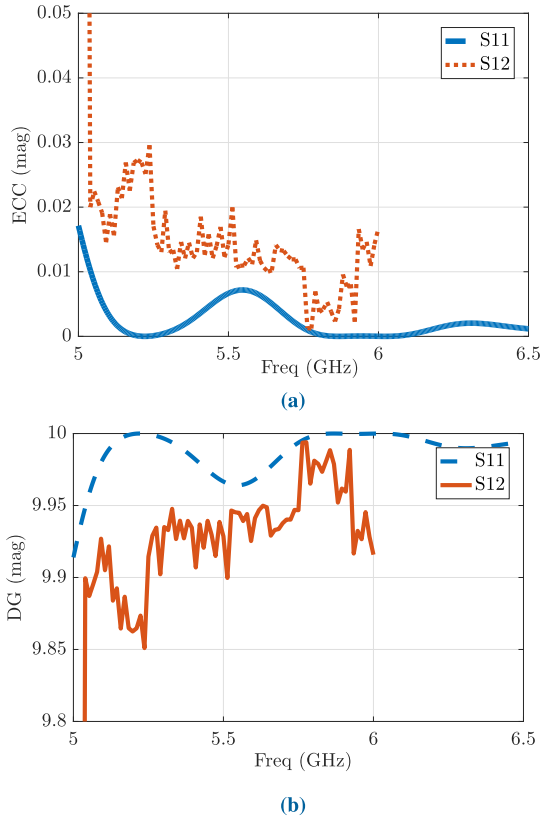

FIGURE 12. Comparison of Simulated and Measured: (a) ECC, (b) DG.

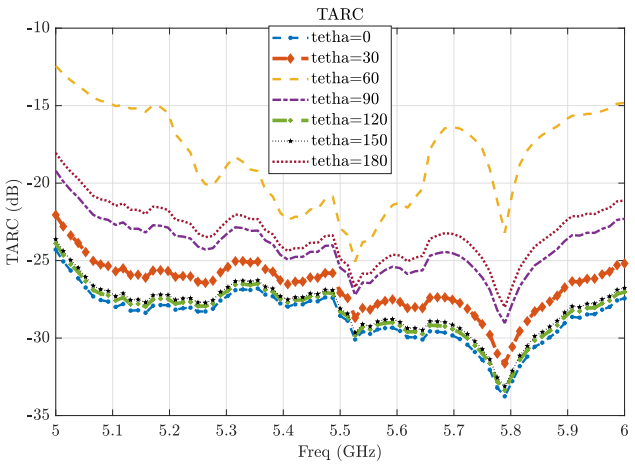

FIGURE 13. Antenna Measured TARC with the variation of theta.

good pattern diversity among the operating frequency band. In addition, the simulated and measured DG is observed to be more than 9.9 dB for the operating frequency range according to Fig.12b. Besides; the measured and simulated values of TARC observed with the variation of input phase are computed using the S-parameters and shown in Fig.13. The TARC graphs demonstrate that the values of TARC are less than −15 dB for the entire band. One can sum that the operating bandwidths of the TARC at all phase angles cover the operating band with stable resonant characteristics which yield a good isolation performance.

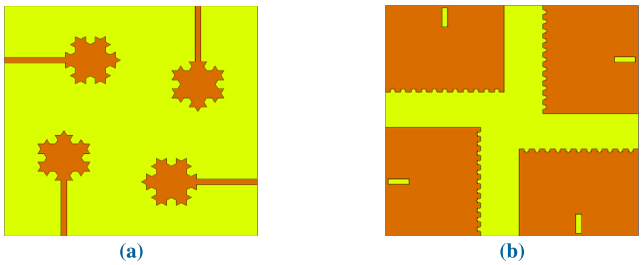

FIGURE 14. MIMO Antenna configuration (MIMO Antenna 1): (a) Front view, (b) back view.

V. 2 × 2 ELEMENTS ANTENNA (SPATIAL AND POLARIZATION DIVERSITIES)

It is worth noticing that the channel capacity is proportional to the antenna number on a MIMO system. For instance, this section analyses the performance of four elements MIMO antenna. The geometrical configuration of the first proposed four elements MIMO antenna is shown in Fig.14. The design is printed on 1.6 mm thick 95×95 mm^2 substrates, it is worthy to mention that the space between adjacent elements is 15 mm in all projected MIMO configurations. As per the observation, all the axis of the radiating elements is placed with angle of 90 and the spacing between the radiators are optimized in such a way that a compact geometry with minimum mutual coupling is achieved.

The reflection coefficients of four Koch fractal MIMO (Antenna 1) are presented in Fig.15a. It is found that the antenna covers the desired frequency band of 5.9 GHz with a peak Sii (i=1, 2, 3, 4) of −50 dB. The transmission coefficient characteristics for the four Koch fractal MIMO Antenna 1 as a function of frequency are plotted in Fig.15b. It is observed that the simulated S21, S41, S12, S32, S23, S43, S14, and S34 parameters are −19.75 dB whilst S31, S13, S24, and S42 parameters are −22 dB at 5.9 GHz.

VI. ISOLATION ENHANCEMENT USING DNG METAMATERIALS

The isolation of the proposed MIMO antenna is pretty poor in the desired frequency. To reduce the mutual coupling between MIMO elements two new broadside coupled square SRR structures are analyzed and attached on both ground plane and between radiators.

A. DNG METAMATERIAL UNIT CELL LA CELLULE ECSRR A COUPLAGE LATERAL, (MMT 1)

The first proposed unit cell is a broadside-electrically coupled metamaterial structure composed of two open electrically coupled conducting square rings which are etched at both sides of a dielectric substrate and with the gaps in opposite positions named MTM1. Figure Fig.16a depicts the side and 3D views of the MTM1 unit cell designed at 5.9 GHz. The length of the unit cells along the z-axis was token in order to be identical with the antenna substrate thickness. Fig.16b shows the simulated results of the reflection coefficients S11/S22 and transmission coefficients S21/S12 of the

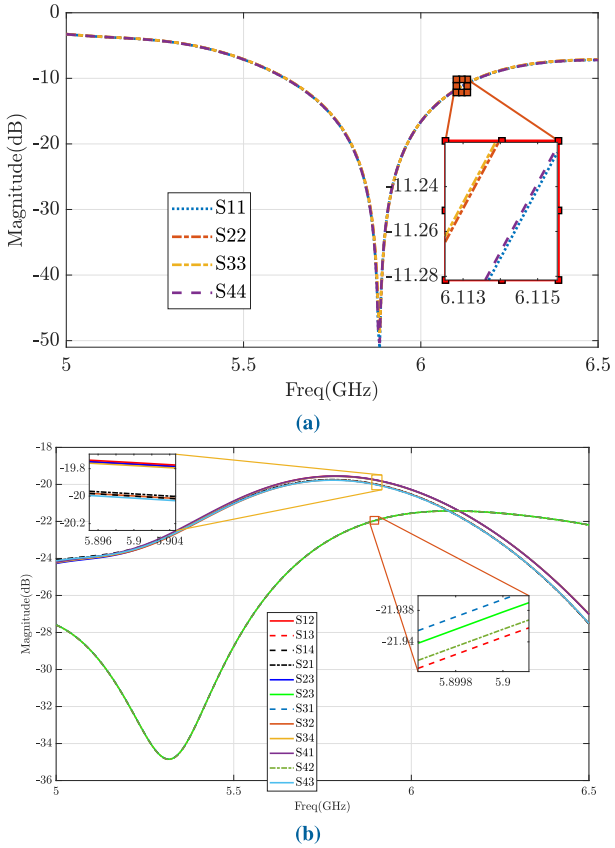

FIGURE 15. (a) MIMO Antenna 1 simulated reflection coefficients, (b) MIMO Antenna 1 simulated transmission coefficients.

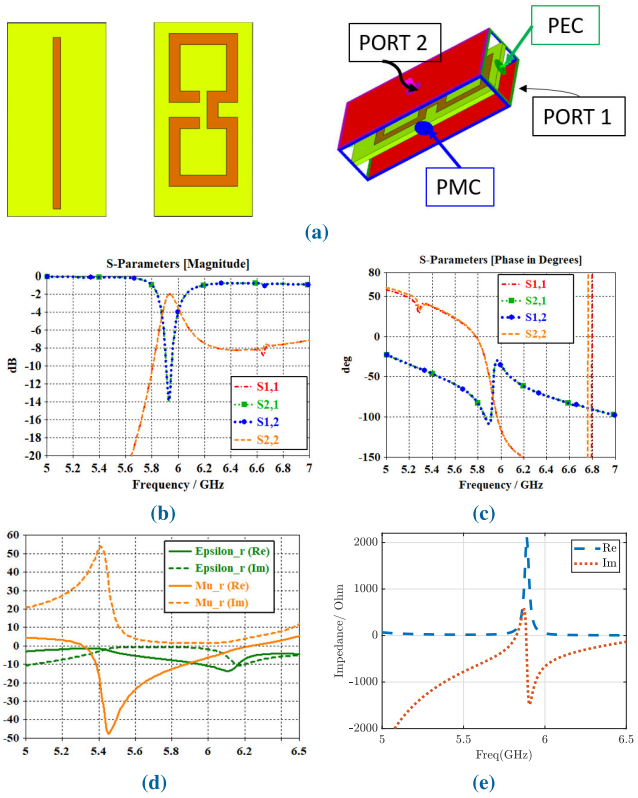

FIGURE 16. (a) Illustration of first DNG metamaterial unit cell and simulation set-up (MTM1), (b) simulated S-parameters, (c) reflection phase, (d) extracted characteristics, and (e) unit cell Impedance.

suggested broadside-electrically coupled metamaterial unit cell besides of the reflection phase (Fig.16c), which is very important to be close to zero at the resonant frequency. The effective relative permittivity and permeability of the metamaterial unit cell have been retrieved utilizing the method proposed in [23]. The extracted characteristics are plotted in Fig.16d, it can be observed that the real parts of the effective relative permittivity and permeability are simultaneously negative in a frequency range from 5.4 to 6.2 GHz. The MTM1 unit cell present a high impedance around the operating frequency (Fig.16e). Therefore, the proposed metamaterial structure could be used to reduce the mutual coupling between the adjacent MIMO antenna elements.

B. DOUBLE NEGATIVE METAMATERIAL COMPOSED OF WIRE STRIPS/EC-SRR, (MTM2)

The second proposed metamaterial unit cell (MTM2)is designed and simulated using CST microwave studio software. The reflection property of proposed unit cells was investigated by setting up the perfect magnetic conductor (PMC) boundary condition for the XY plane, whilst the perfect electric conductor (PEC) boundary conditions are applied for the YZ plane, and the waveguide ports are applied in the Z direction. Fig.17a depicts the front, back, and 3D views of the second designed unit cell for the V2X frequency band. As seen from the simulated results (S-parameters, reflection phase, the dielectric constant ϵ), and the permeability (μ)) as illustrated in Fig.17b, Fig.17c, Fig.17d and Fig.17e that the extracted effective permeability and permittivity of the designed unit cell are negative with very high impedance around 5.9 GHz frequency band. One can also note that the proposed metamaterial achieves a bandwidth of both the permittivity and permeability values are negative of 800 MHz (from 5.4 to 6.2 GHz).

C. RETURN LOSS (S11/S22/S33/S44) AND ISOLATION ANALYSIS OF MIMO ANTENNA 1 WITH THE MTM1 AND MTM2 CELLS

The first proposed DNG structure is inserted on between the adjacent MIMO elements as appears in Fig.18, and Fig.19. The reflection and transmission coefficients of the four elements MIMO antenna with the first suggested metamaterial structure (MIMO Antenna 2) are plotted in Fig.20a, and Fig.20b, respectively. From these figures, one can see that the return loss of the antenna at the 5. 9 GHz frequency is −30 dB. Besides, the simulated transmission coefficients are lower than −40dB at 5.9 GHz. It is observed that isolation between port-4/ port-2, and port-1/port-3 is of 35 dB. In addition, it is observed that the isolation between port-1/port-2 and port-4/port-3 is up to −40dB. Meanwhile, significant isolation is obtained for port-1/port-4 and port-2/port-3. Hence,

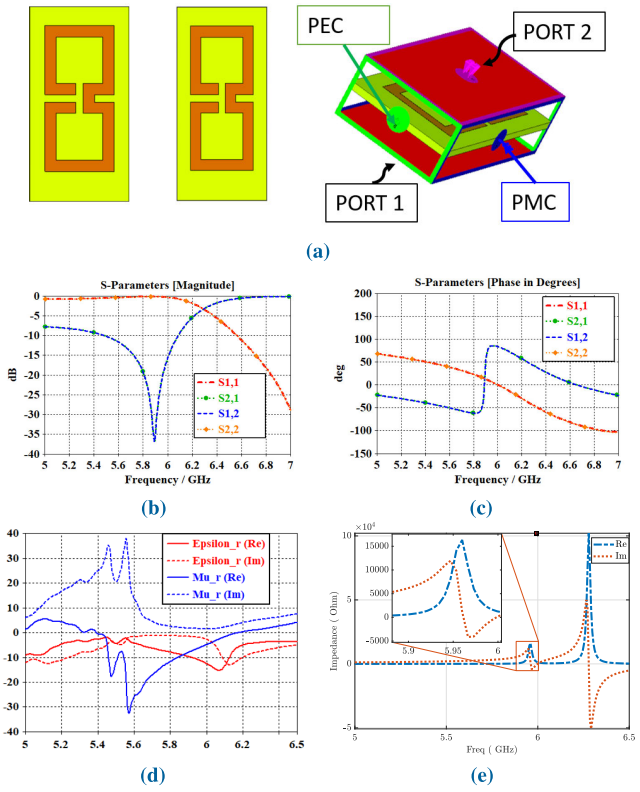

FIGURE 17. (a) Illustration of first DNG metamaterial unit cell and simulation set-up (MTM2), (b) simulated S-parameters, (c) reflection phase, (d) extracted characteristics (ϵ, μ), and (e) unit cell Impedance.

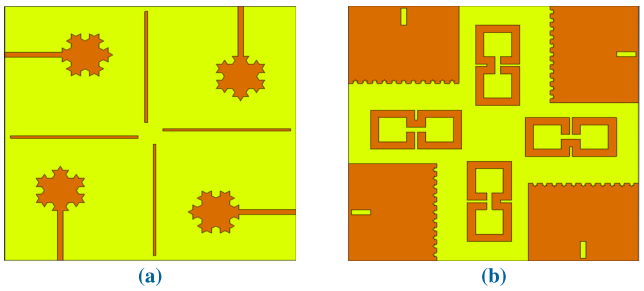

FIGURE 18. MIMO Antenna 2: (a) Front views, (b)Back view.

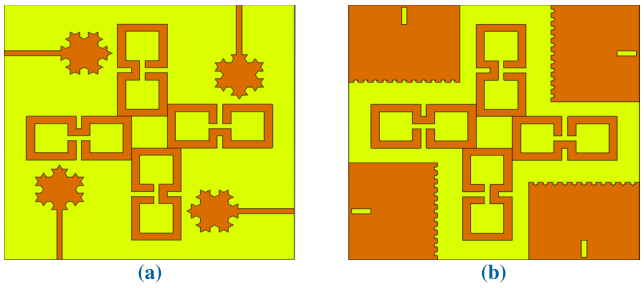

FIGURE 19. MIMO Antenna 3: (a) Front views, (b)Back view.

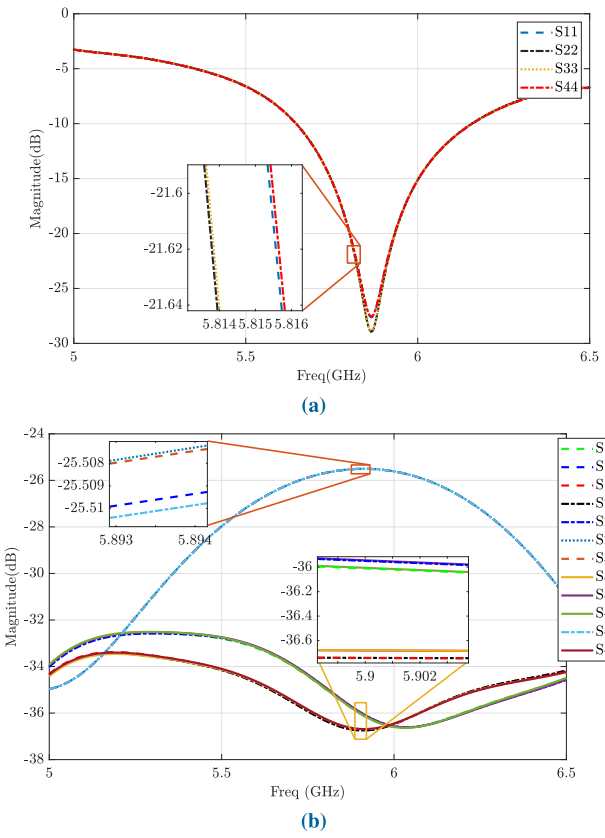

FIGURE 20. (a) MIMO Antenna 2 simulated reflection coefficients, (b) MIMO Antenna 2 simulated transmission coefficients.

the minimum obtained mutual coupling between the suggested MIMO antennas is below -35 dB. Then, one can conclude that the use of the proposed metamaterial cells considerably increases the isolation of the MIMO antenna with a good impedance matching. The characterization of the Koch MIMO antenna with the second suggested metamaterial structure (MIMO Antenna 3 as illustrated in Fig.19) is carried out by plotting the reflection coefficients Sii (with i=1, 2, 3, 4) and transmission coefficients Sij (with i‘#j) using CST MWS software. Fig.21a provides S-parameter graphs, it is well observed that the reflection coefficients Sii cover the operating bandwidth of 5.6-6.19 GHz with a peak value of −40dB at 5.9 GHz. Besides, Fig.21b exhibits the transmission coefficient curves. It is observed that isolation between adjacent and opposite ports is less than −35dB. The transmission coefficient results validate the isolation enhancement between the MIMO antenna elements after incorporation of the metamaterial cells.

VII. DIVERSITY ANALYSIS OF THE THREE MIMO ANTENNA CONFIGURATIONS

Subsequently to observe the three proposed MIMO antenna performance, a detailed analysis of MIMO parameters, such as ECC, D.G, M.E.G, CCL, and TARC, is discussed in detail.

In the current work, the ECC is computed through the S-parameters way. Ideally, ECC should be zero but for uncorrelated diversity, the values should lie at ECC < 0.5. The graph in Fig.22 explores a comparative analysis of the three MIMO configuration ECC performance. One can denote from these graphs that the proposed antenna configurations have ECC

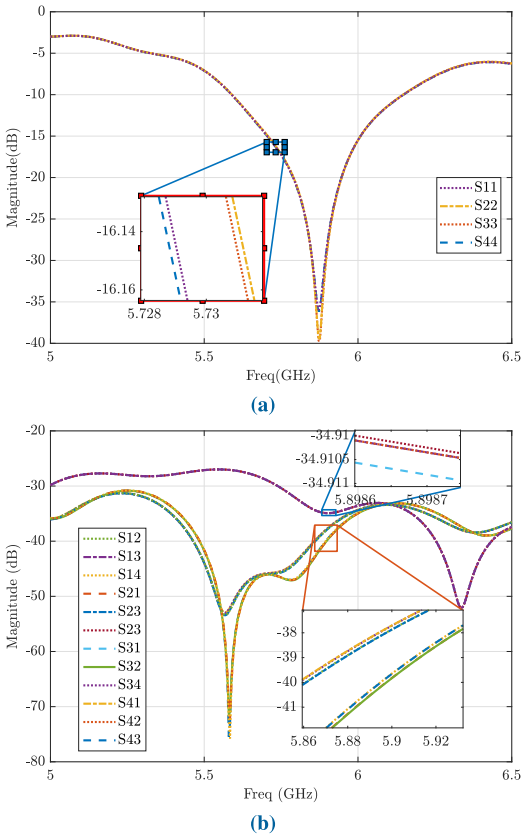

FIGURE 21. (a) MIMO Antenna 3 simulated reflection coefficients, (b) MIMO Antenna 3 simulated transmission coefficients.

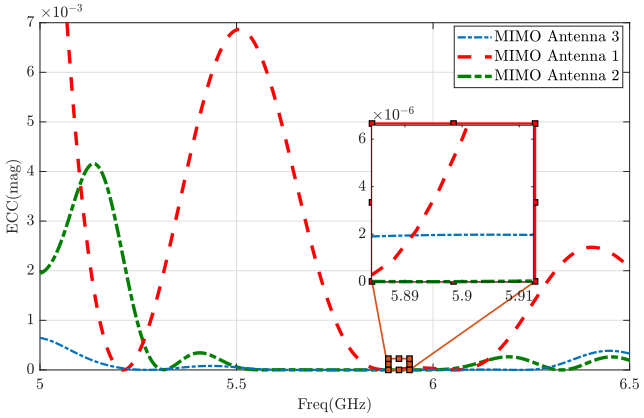

FIGURE 22. ECC Comparison of three MIMO antenna.

lower than 0.001 for the desired frequency range, hence, a very low correlation is observed at the 5.9 GHz band due to uncorrelated patterns because of the ports orthogonal polarization. Whereas, the simulated DG is mentioned in Fig.23. The DG values>9.999 in the frequency band from 5.25-6.5 GHz. This result indicates the low correlation between the MIMO antenna elements and this could be explained by the mean of polarization diversity as well as the metamaterial cells.

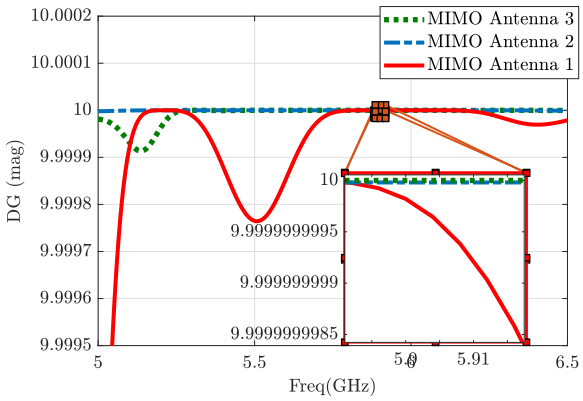

FIGURE 23. DG Comparison of three MIMO antenna.

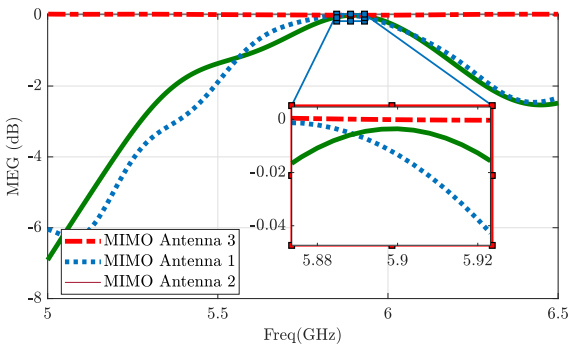

FIGURE 24. MEG Comparison of three MIMO antenna.

Mean effective gain (MEG) is a characteristic that includes antenna radiation power pattern, antenna efficiency, and propagation effects. For optimum antenna design, MEG values should be equal for all the antenna elements. One can observe from Fig.24 that the MEG values are equal for all ports as well as k (equation 8) is less than 3dB within operating frequency and close to zero at 5.9 GHz. This makes the antenna a good candidate to be implemented in the real multipath environment. For further behavior analysis, the simulated CCL curves are illustrated in Fig.25. The values of CCL are recorded to be lower than 0.3 for the operating frequency range. It is apparent that at 5.9 GHz, CCL reaches a value lower than 0.25 b/s/Hz for the application band which makes the proposed MIMO antenna configurations a good choice for practical vehicular communications.

TARC takes into account impedance matching, mutual coupling, and radiation efficiency under the random phase excitations at input ports. Indeed, higher mutual coupling leads to worse TARC. In the proposed system the TARC is calculated using (10) between Port-1 and Port-2 for various input phases, the simulated TARC curves are depicted in Fig.26a, Fig.26b, and Fig.26c for MIMO antenna 1, MIMO Antenna 2 and MIMO Antenna 3 respectively. One can easily notice that the incoming signal phases have a small impact on the TARC at the operating frequency, especially at 5.9 GHz, besides the MIMO Antenna 3 show a stable TARC

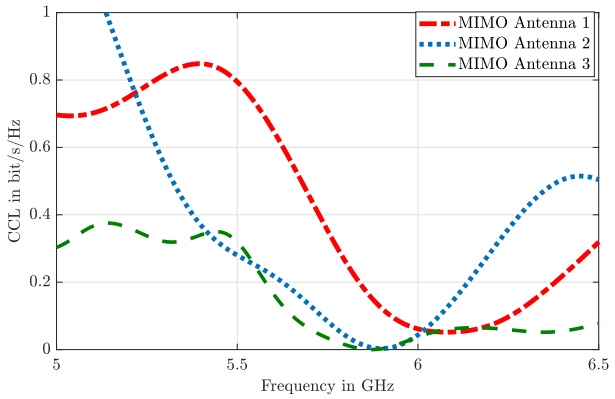

FIGURE 25. CCL Comparison of three MIMO antenna.

TABLE 1. Various MIMO antenna fields' distribution comparison.

The Field in dB (A/m)			
	MIMO Antenna 1	MIMO Antenna 2	MIMO Antenna 3
Source	28	28	28
Zone A	9.72	-13.33	3.26
Zone B	6.43	0.56	10.26
Zone C	6.23	1.29	2.4
Zone D	7.22	-22.52	-13
Zone E	1.10	-8	0.77
Zone F	8.85	-18.2	1.41
Zone G	10.17	-10	2.25

performance around the 5.9 GHz. Please note that the lower correlation between ports in the MIMO antenna could be the reason to obtain a family of TARC graphs less susceptible to the phase variations of the input signals. Furthermore, it is apparent based on the suggested MIMO antenna 3 S-parameters analysis, one can assumes that the transmission coefficients must be smaller than reflection coefficients in order to reduce significantly the effect of the phase of the incoming signals.

VIII. EFFECT OF SUGGESTED METAMATERIAL CELLS ON RADIATION PATTERN

It is evident that the mutual coupling alters the antenna pattern. So, to show the mutual coupling effect on antenna patterns, the three studied MIMO antennas simulated 3D radiation patterns if all ports are excited simultaneously as well as surface current density if port 1 is the only exciting port at 5.9 GHz are projected and analyzed in this section.

A further investigation included comparison between surface current density of the three suggested MIMO antennas at same input phase. Fig.28 provides a study of surface current density distribution which is simulated at 5.9 GHz by exciting port-1 while ports 2/ 3/4 were terminated with a matched load. As expected, the maximum surface current density is strongly concentrated within/around the fed line, patch edges

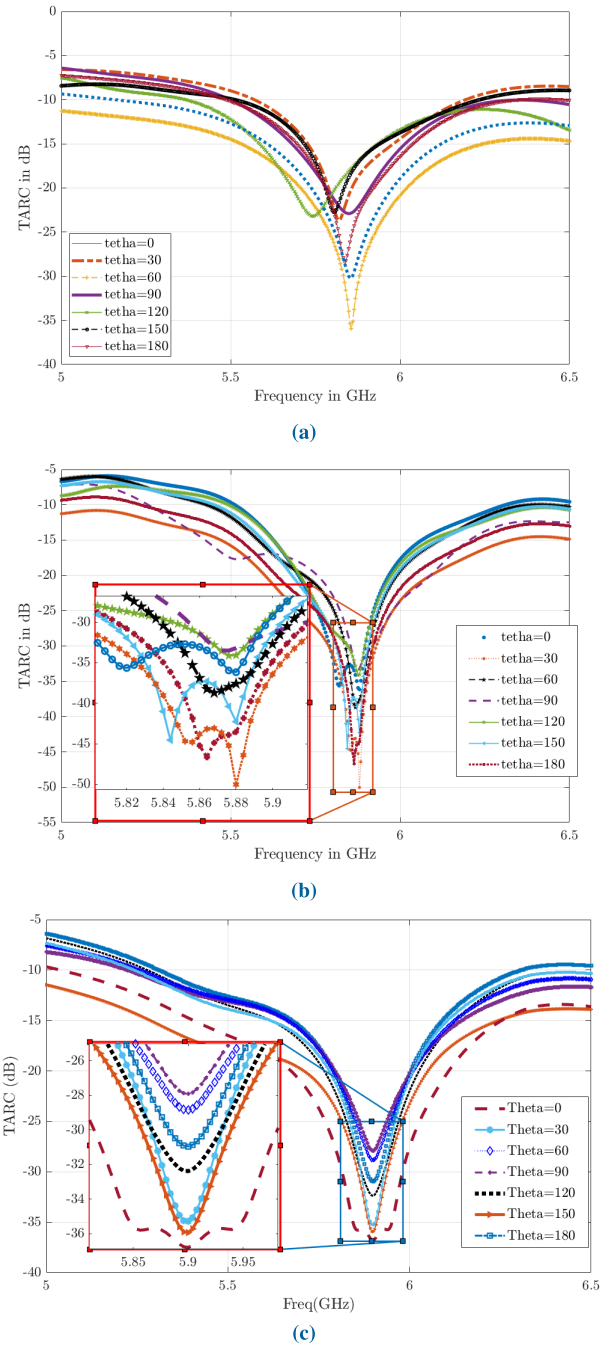

FIGURE 26. Simulated TARC: (a) MIMO Antenna 1, (b) MIMO Antenna 2, (c) MIMO Antenna 3.

and ground plane bounds with negligible density in other antenna parts. Moreover, it is clearly seen that the induced surface current density in the feeding line at port-2, port-3 and port-4 as well as the induced current on the ground plane edges of the adjacent antennas (port-2 and port-4) is high when the metamaterial cells are absent. So then, it is worth to mention that by placing metamaterial cells in between the MIMO antenna adjacent elements the surface current is mainly concentrated in addition to the patch and ground plane edges and through the metamaterial structures. The one can

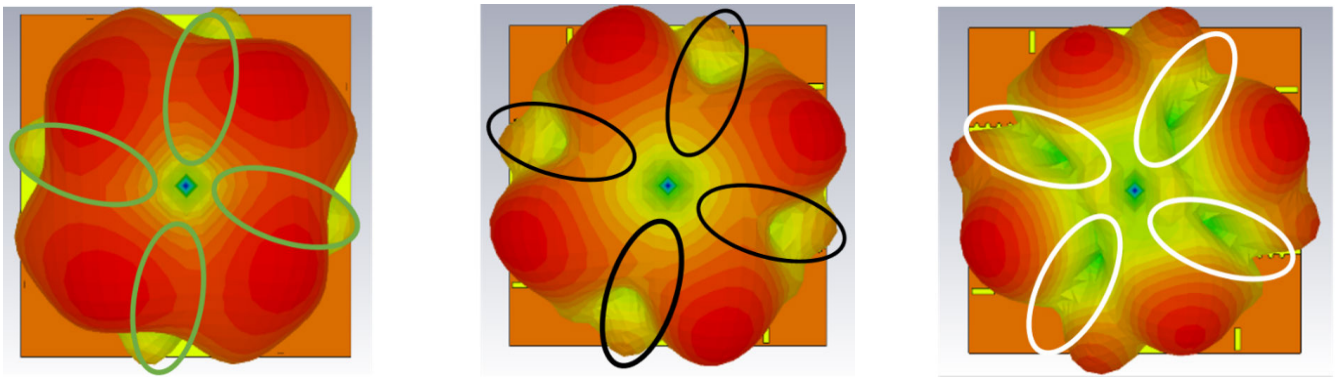

FIGURE 27. Simulated 3D radiation pattern: (a) MIMO Antenna 1, (b) MIMO Antenna 2, (c) MIMO Antenna 3.

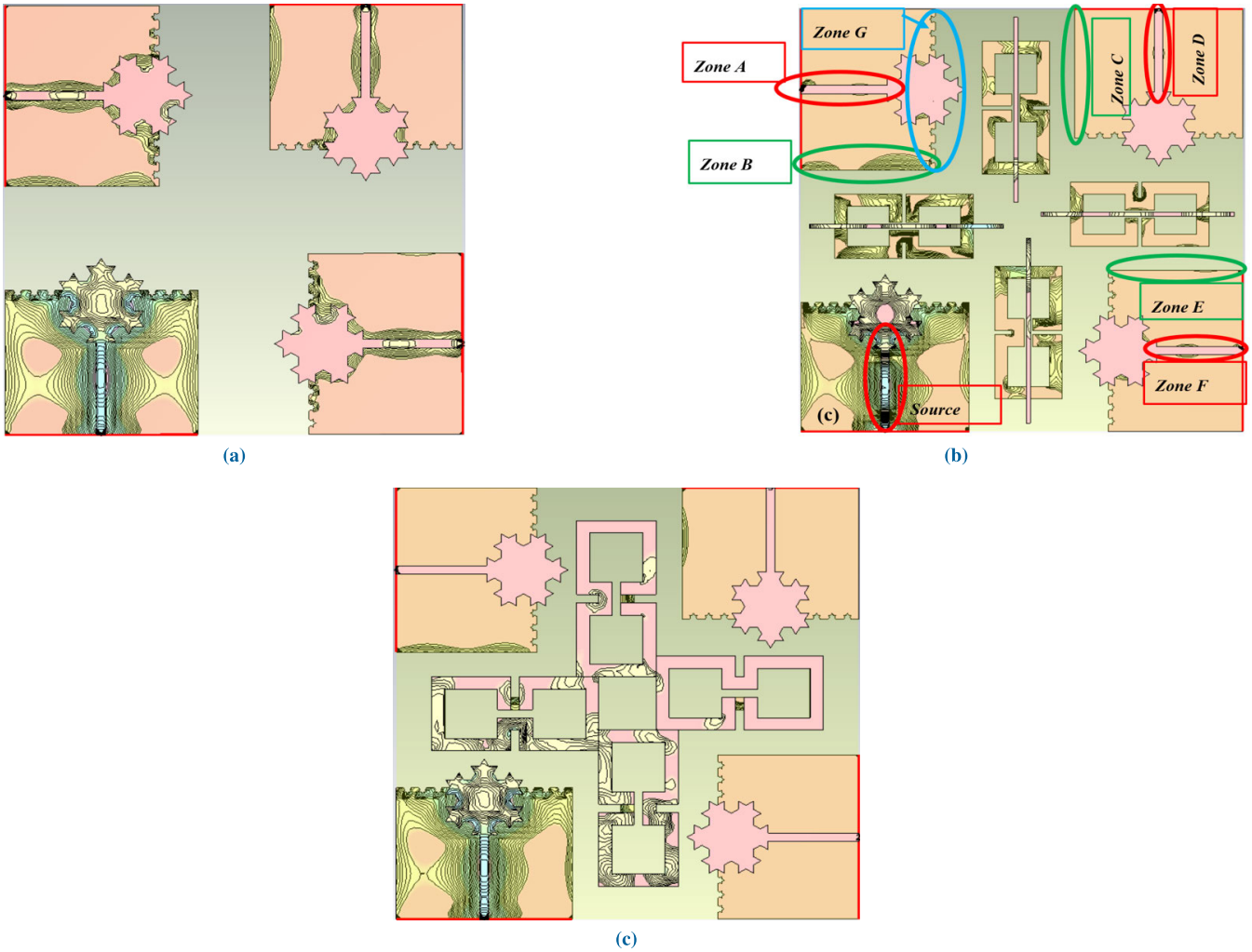

FIGURE 28. Surface current density distribution: (a) MIMO Antenna 1, (b) MIMO Antenna 2, (c) MIMO Antenna 3.

conclude that the ability to forbid the propagation of surface waves afterward is the main key to provide an enhancement of the mutual coupling between the MIMO antenna elements. Another attempt which may be interesting to study more in-depth the metamaterial behavior is the antenna field distribution. As the Table.1 lists, the field values have been derived and compared for the three investigated MIMO antennas. The performed comparison ensures the crucial role of the

TABLE 2. Comparison of the proposed antennas with previous works.

Ref	Dim. (mm^2)	No of Elements	Isolation (dB)	ECC	Technique
[26]	121.8 × 45	2	> 20	< 0.1	ground plane shape modification
[28]	92 × 27	2	> 20	< 0.05	Metamaterial
[29]	22 × 32	2	> 19	< 0.17	Defected ground plane
[30]	40 × 20	2	> 20	< 0.1	Steped ground plane
[32]	——	4	25.3-32.6	< 0.34	SRR loaded with transmission line
[33]	47.5 × 40	2	>15	< 0.05	Metamaterial
[37]	50 × 55	2	> 26;	< 0.28	large distance between elements
This work	single : 40 × 40 MIMO Antenna 1: 95× 95 MIMO Antenna 2: 90×90 MIMO Antenna 3: 90×90	4	> 30	< 0.02	Metamaterial

metamaterial structures in MIMO antenna diversity performance quality improvement. A comparison of the proposed MIMO antenna configurations with the some other same kinds of MIMO antenna systems from the literature is given in Table.2.

IX. CONCLUSION

In this research article, a new compact single, two elements, four elements MIMO antenna based on Koch fractal geometry are characterized at sub 6GHz 5G for vehicular communications. To reduce the mutual coupling among MIMO antenna ports, the diversity polarization technique was employed. Additionally, we introduced two left handed metamaterial structures to enhance the isolation and the diversity features of the 2 × 2 MIMO antenna. The metamaterial shapes are based on broadside/electrically coupled square ring resonators and stub which are installed between MIMO antenna adjacent elements. The reflection coefficients, and isolation besides the diversity performance in term of ECC, DG, MEG, TARC and CCL are analyzed. From this analysis it was determined that the projected MIMO antenna configurations offer good diversity performance. However, the obtained parameters were as follows: reflection coefficients lower than $30dB$ at the resonant frequency for all configurations, isolation of -20 dB and $> -35dB$. Before and after introducing the metamaterial cells, MEG close to 0 dB for all configurations, and TARC values below $-20dB$ that are slightly affected by the incoming excitations phases. Nevertheless, the reflection coefficients are quite badly affected by introducing the metamaterial cells. In contrast, the MIMO diversity parameters as well as isolation were all considerably enhanced with the addition of the metamaterial structures between MIMO adjacent elements. Moreover, the behavior of the MIMO antenna with and without metamaterials is analyzed by comparing the 3D radiation pattern and current density of the three projected 2 × 2 MIMO configurations. In summary, we can affirm that the MIMO antenna configurations presented in this work are good proposal in sub 6 GHz 5G and IEEE 802.11p based vehicular applications.

REFERENCES

[1] P. K. Singh, S. K. Nandi, and S. Nandi, "A tutorial survey on vehicular communication state of the art, and future research directions," *Veh. Commun.*, vol. 18, Aug. 2019, Art. no. 100164. [Online]. Available: http://www.sciencedirect.com/science/article/pii/S2214209618300901, doi: 10.1016/j.vehcom.2019.100164.

[2] D.-T. Do, T.-T.-T. Nguyen, C.-B. Le, and J. W. Lee, "Two-way transmission for low-latency and high-reliability 5G cellular V2X communications," *Sensors*, vol. 20, no. 2, p. 386, Jan. 2020, doi: 10.3390/s20020386.

[3] J. Narrainen, "Performance evaluation of vehicle radiofrequency communication systems: Contribution to the modelling approach," M.S. thesis, INSA de Rennes, Rennes, France, 2017.

[4] N. Alexandrov, *Antenna Arrays and Automotive Applications*. New York, NY, USA: Springer, 2013.

[5] A. Attia, A. ElMoslimany, A. El-Keyi, T. ElBatt, F. Bai, and C. Saraydar, "MIMO vehicular networks: Research challenges and opportunities," *J. Commun.*, vol. 7, no. 7, pp. 500–513, Jul. 2012.

[6] T. Kopacz, A. Narbudowicz, D. Heberling, and M. J. Ammann, "Evaluation of automotive MIMO antennas for V2V communication in urban intersection scenarios," in *Proc. 11th Eur. Conf. Antennas Propag. (EUCAP)*, Mar. 2017, pp. 2907–2911, doi: 10.23919/EuCAP.2017.7928476.

[7] L. Ekiz, A. Thiel, O. Klemp, and C. F. Mecklenbräuker, "MIMO performance evaluation of automotive qualified LTE antennas," in *Proc. 7th Eur. Conf. Antennas Propag. (EuCAP)*, Apr. 2013, pp. 1412–1416.

[8] D. Tang, G. Shao, J. Zhou, and H. Kikuchi, "A novel MIMO channel model for vehicle-to-vehicle communication system on narrow curved-road environment," *Wireless Pers. Commun.*, vol. 98, no. 4, pp. 3409–3430, Feb. 2018, doi: 10.1007/s11277-017-5021-6.

[9] N. Kishore, G. Upadhyay, V. S. Tripathi, and A. Prakash, "Dual band rectangular patch antenna array with defected ground structure for ITS application," *AEU, Int. J. Electron. Commun.*, vol. 96, pp. 228–237, Nov. 2018.
[10] M. A. Westrick, "Compact wire antenna array for dedicated short-range communications: Vehicle to vehicle and vehicle to infrastructure communications," Doctoral dissertation, Univ. Toledo, Toledo, OH, USA, 2012.
[11] T. Pujar and M. Ningappa, "Overview of fractal microstrip MIMO antenna for wireless communication," *Int. J. Sci. Eng. Res.*, vol. 10, no. 3, pp. 744–748, Mar. 2019.
[12] S. S. Khade and P. D. Bire, "Fractal MIMO antenna for wireless application," in *Optical and Wireless Technologies: Proceedings of OWT 2018* (Lecture Notes in Electrical Engineering), vol. 546. Singapore: Springer, 2020, pp. 347–356.
[13] P. Bhutani, S. Sagar, and A. Kumar, "Performance analysis of Sierpinski carpet fractal antenna for wireless communication," in *Applications of Computing, Automation and Wireless Systems in Electrical Engineering: Proceedings of MARC 2018* (Lecture Notes in Electrical Engineering). Singapore: Springer, 2019, pp. 749–758.
[14] J. S. Sivia, G. Kaur, and A. K. Sarao, "A modified Sierpinski carpet fractal antenna for multiband applications," *Wireless Pers. Commun.*, vol. 96, pp. 4269–4279, Feb. 2017.
[15] P. Kopyt, B. Salski, P. Zagrajek, D. Janczak, M. Sloma, M. Jakubowska, M. Olszewska-Placha, and W. Gwarek, "Electric properties of graphene-based conductive layers from DC up to terahertz range," *IEEE Trans. THz Sci. Technol.*, vol. 6, no. 3, pp. 480–490, May 2016, doi: 10.1109/TTHZ.2016.2544142.
[16] T. Mondal, S. Samanta, R. Ghatak, and S. R. Bhadra Chaudhuri, "A novel tri-band hexagonal microstrip patch antenna using modified Sierpinski fractal for vehicular communication," *Prog. Electromagn. Res. C*, vol. 57, pp. 25–34, 2015.
[17] A. Gorai, A. Dasgupta, and R. Ghatak, "A compact quasi-self-complementary dual band notched UWB MIMO antenna with enhanced isolation using Hilbert fractal slot," *AEU, Int. J. Electron. Commun.*, vol. 94, pp. 36–41, Sep. 2018.
[18] I. S. Bangi and J. S. Sivia, "Minkowski and Hilbert curves based hybrid fractal antenna for wireless applications," *AEU Int. J. Electron. Commun.*, vol. 85, pp. 159–168, Feb. 2018.
[19] B. K. Soni and R. Singhai, "Design and analysis of Minkowskized hybrid fractal like antenna for multiband operation," *Prog. Electromagn. Res. Lett.*, vol. 80, pp. 117–126, 2018, doi: 10.2528/PIERL18092904.
[20] V. Tharani, N. S. Priya, and A. Rajesh, "Design of inside cut Von Koch fractal UWB MIMO antenna," *IOP Conf. Ser., Mater. Sci. Eng.*, vol. 263, no. 5, 2017, Art. no. 052043, doi: 10.1088/1757-899x/263/5/052043.
[21] H. Rajabloo, V. A. Kooshki, and H. Oraizi, "Compact microstrip fractal Koch slot antenna with ELC coupling load for triple band application," *AEU, Int. J. Electron. Commun.*, vol. 73, pp. 144–149, Mar. 2017.
[22] Y. K. Choukiker and S. K. Behera, "Wideband frequency reconfigurable Koch snowflake fractal antenna," *IET Microw., Antennas Propag.*, vol. 11, no. 2, pp. 203–208, Jan. 2017.
[23] J. Ali, S. Abdulkareem, A. Hammoodi, A. Salim, M. Yassen, M. Hussan, and H. Al-Rizzo, "Cantor fractal-based printed slot antenna for dual-band wireless applications," *Int. J. Microw. Wireless Technol.*, vol. 8, no. 2, pp. 263–270, Mar. 2016.
[24] F. Ez-Zaki, H. Belahrach, and A. Ghammaz, "Broadband microstrip antennas with Cantor set fractal slots for vehicular communications," *Int. J. Microw. Wireless Technol.*, vol. 13, no. 3, pp. 295–308, Apr. 2021.
[25] S. Bhatt, P. Mankodi, A. Desai, and R. Patel, "Analysis of ultra wideband fractal antenna designs and their applications for wireless communication: A survey," in *Proc. Int. Conf. Inventive Syst. Control (ICISC)*, Jan. 2017, pp. 1–6, doi: 10.1109/ICISC.2017.8068736.
[26] A. Peristerianos, A. Theopoulos, A. G. Koutinos, T. Kaifas, and K. Siakavara, "Dual-band fractal semi-printed element antenna arrays for MIMO applications," *IEEE Antennas Wireless Propag. Lett.*, vol. 15, pp. 730–733, 2016, doi: 10.1109/LAWP.2015.2470681.
[27] C. A. Ballanis, *Antenna Theory: Analysis and Design*. New York, NY, USA: Wiley, 2016.
[28] S. Adham, "Investigation of integrated decoupling methods for MIMO antenna systems. Design, modelling and implementation of MIMO antenna systems for different spectrum applications with high port-to-port isolation using different decoupling techniques," Ph.D. dissertation, Univ. Bradford, Bradford, U.K., 2019. [Online]. Available: http://hdl.handle.net/10454/18427
[29] G. Irene and A. Rajesh, "A penta-band reject inside cut Koch fractal hexagonal monopole UWB MIMO antenna for portable devices," *Prog. Electromagn. Res. C*, vol. 82, pp. 225–235, 2018, doi: 10.2528/PIERC18020604.
[30] R. Sampath and K. T. Selvan, "Compact hybrid Sierpinski Koch fractal UWB MIMO antenna with pattern diversity," *Int. J. RF Microw. Comput.-Aided Eng.*, vol. 30, no. 1, Jan. 2020, Art. no. e22017.
[31] S. Kumar and R. Kumari, "Bandwidth and gain-enhanced composite right/left-handed antenna for ultra-wideband applications," *Int. J. RF Microw. Comput.-Aided Eng.*, vol. 30, no. 3, Mar. 2020, Art. no. e22095.
[32] A. Bellary, K. Kandasamy, and P. H. Rao, "Mitigation of mutual coupling in 2 × 2 dual slant polarized MIMO antennas using periodic array of SRRs loaded with transmission line for LTE band 40," *Int. J. RF Microw. Comput.-Aided Eng.*, vol. 30, no. 12, Dec. 2020, Art. no. e22454.
[33] C. Wang, X. Yang, and B. Wang, "A metamaterial-based compact broadband planar monopole MIMO antenna with high isolation," *Microw. Opt. Technol. Lett.*, vol. 62, no. 9, pp. 2965–2970, Sep. 2020, doi: 10.1002/mop.32406.
[34] Y. Guo, J. Zhao, Q. Hou, and X. Zhao, "Omnidirectional broadband patch antenna with horizontal gain enhanced by epsilon-snegative metamaterial superstrate," *Microw. Opt. Technol. Lett.*, vol. 62, no. 2, pp. 778–788, Feb. 2020.
[35] J. W. Krzysztofik and F. Brambila, "Fractals in antennas and metamaterials applications," in *Fractal Analysis: Applications in Physics Engineering and Technology*. IntechOpen, 2017, pp. 953–978, doi: 10.5772/intechopen.68188.
[36] A. D. Tadesse, O. P. Acharya, and S. Sahu, "Application of metamaterials for performance enhancement of planar antennas: A review," *Int. J. RF Microw. Comput.-Aided Eng.*, vol. 30, no. 5, pp. 1–20, May 2020.
[37] A. Yacoub, M. Khalifa, and D. N. Aloi, "Compact 2 × 2 automotive MIMO antenna systems for sub-6 GHZ 5G and V2X communications," *Prog. Electromagn. Res. B*, vol. 93, pp. 23–46, 2021.

FATIMA EZ-ZAKI received the B.Sc. degree in industrial computer, electronic, electrotechnical and automatic and the M.Sc. Tech. (Eng.) in electrical engineering from Cadi Ayyad University, Marrakesh, Morocco, in 2015 and 2017, respectively, where she is currently pursuing the Ph.D. degree with the Department of Applied Physics. Her research interests include telecommunications, fractal antennas, microwave, metamaterial, and vehicular communications.

HASSAN BELAHRACH received the B.S. degree in electrical and electronics engineering from Mohamed V University, Rabat, Morocco, in 1986, the M.S. degree in electronics and microelectronics engineering and the Ph.D. degree in microelectronics and technology from Bordeaux I University, France, in 1987 and 1990, respectively, and the Ph.D. degree in microelectronics and telecommunication from Cadi Ayyad University, Marrakesh, Morocco, in 2001. He is currently a Full University Professor of analog and digital electronics with Royal Air Academy, Marrakesh. His research interest includes the analysis and design packaging of very high-speed CMOS suitable for telecommunication applications.

ABDELILAH GHAMMAZ received the Ph.D. degree in electronics engineering from the National Polytechnic Institute of Toulouse (ENSEEIHT), Toulouse, France, in 1993. In 1994, he went back to Cadi Ayyad University, Marrakesh, Morocco. Since 2003, he has been a Professor with the Faculty of Sciences and Technology, Cadi Ayyad University, Marrakesh. His research interests include electromagnetic compatibility and antennas.

SAROSH AHMAD (Student Member, IEEE) received the bachelor's degree in electrical engineering with specialization in telecommunication engineering from the Department of Electrical Engineering and Technology, Government College University Faisalabad (GCUF), Pakistan, in 2021. He is currently pursuing the master's degree in advanced communication technology with the Department of Signal Theory and Communications, Universidad Carlos III de Madrid (UC3M), Madrid, Spain. He has published 15 conference papers, 30 high indexed international journals, and five book chapters by Springer. His research interests include radio-frequency (RF) circuit design, radiofrequency identification (RFID), signals and systems, wearable and flexible antennas, metamaterial-based antennas, implantable antennas, multi-input-multi-output (MIMO) antennas, mm-wave antennas, 5G antennas, antenna arrays, dielectric resonator antennas (DRAs), photonic antennas, fluidic antennas, antenna for the Internet of Things applications, ultra-wideband (UWB) antennas, wideband antennas, reconfigurable antennas, substrate integrated waveguide (SIW) antennas, circularly polarized antennas, terahertz antennas, rectennas for energy harvesting applications, bandpass filters, half- and full-wave filter antennas, active sensors, and the IoT-based communication devices. He is a member of the IEEE Antennas and Propagation Society (APS). During the graduation, he received the fully funded PEEF Scholarship Award from the Prime Minister of Pakistan and the Silver Medal in the bachelor's program. During his volunteer-ship, he contributed himself as a Branch Treasurer at the IEEE GCUF, Faisalabad Subsection, for two years. After the graduation, he again received the fully funded Erasmus Grant Scholarship for the master's program in Madrid. During the graduation research period, he has participated in four international IEEE conferences over the world, where he has presented ten articles mostly in oral presentations. He has presented his two articles in the International Turkish Conferences where he has got the Best Paper Award, one article in the International Moroccan Conference Proceedings and one article in IEEE EuCAP22. He has served as a Volunteer for the 16th IEEE European Conferences on Antennas and Propagations. He has been selected for the fully funded MITACS Internship Program in the nationally ranked University of Canada called Carleton University where he is currently a Researcher in the field of massive MIMO antennas.

ASMA KHABBA received the B.Sc. degree in physics and the master's degree in control, industrial computing, signals and systems from Cadi Ayyad University, Marrakesh, Morocco, in 2015 and 2017 respectively, where she is currently pursuing the Ph.D. degree in telecommunication and signal processing. Her research interests include 5G antenna, microwave/millimeter wave antenna, phased array, and MIMO antenna.

KHAOULA AIT BELAID received the B.S. degree in industrial computer, electronic, electrotechnical and automatic, the M.S. degree in electrical engineering, and the Ph.D. degree in electrical engineering and telecommunications from Cadi Ayyad University, Marrakesh, Morocco, in 2012, 2014, and 2020, respectively. Her research interests include the analysis and design packaging of very high-speed CMOS, modeling 3D structures based on TSVs, and modeling noises in microelectronics systems.

ADNAN GHAFFAR received the B.Sc. degree in computer engineering from Bahauddin Zakariya University (BZU) Multan, Pakistan, in 2010, and the M.E. degree in circuits and systems from Lanzhou Jiaotong University, Lanzhou, China, in 2015. He is currently pursuing the Ph.D. degree in electrical and electronics engineering with the Auckland University of Technology, Auckland, New Zealand. His research interests include RF circuits, reconfigurable antenna, embedded systems, metasurface antenna, flexible, and wearable antenna design.

MOUSA I. HUSSEIN (Senior Member, IEEE) received the B.Sc. degree in electrical engineering from West Virginia Tech, Montgomery, WV, USA, in 1985, and the M.Sc. and Ph.D. degrees in electrical engineering from the University of Manitoba, Winnipeg, MB, Canada, in 1992 and 1995, respectively. From 1995 to 1997, he was with the Research and Development Group, Integrated Engineering Software Inc., Winnipeg, involved in developing EM specialized software based on the boundary element method. In 1997, he joined the Faculty of Engineering, Amman University, Amman, Jordan, as an Assistant Professor. He is currently a Professor with the Department of Electrical Engineering, United Arab Emirates University. He has more than 100 publications in international journals and conferences. He has supervised several M.Sc. and Ph.D. students. His current research interests include computational electromagnetics, electromagnetic scattering, antenna analysis and design, metamaterial and applications, and material/bio-material characterization, and sensor design for bio applications.